

Microwave absorption of supercooled clouds and implications for the dielectric properties of water

Christian Mätzler,¹ Philip W. Rosenkranz,² and Jan Cermak³

Received 30 March 2010; revised 3 August 2010; accepted 24 August 2010; published 7 December 2010.

[1] The absorption of liquid clouds was determined in the frequency range from 21 to 31 GHz and over the temperature range from 246 to 279 K. The information was derived from continuous surface-based microwave and infrared radiometer observations at Bern, Switzerland, from 2006 to 2010 and using satellite data for cloud-top temperature. The results indicate that common dielectric models of liquid water are inaccurate at temperatures below 265 K, possibly owing to the poor representation of the main relaxation frequency of water. The best agreement with our observations is found for a model published in report form in 1995. Part of the scatter in the temperature dependence of the analyzed data can be explained by correlated fluctuations in water vapor and liquid water. The results are relevant for remote sensing of supercooled clouds using passive and active microwave techniques and, more generally, for the physics of water.

Citation: Mätzler, C., P. W. Rosenkranz, and J. Cermak (2010), Microwave absorption of supercooled clouds and implications for the dielectric properties of water, *J. Geophys. Res.*, 115, D23208, doi:10.1029/2010JD014283.

1. Introduction

[2] Microwave radiometers are used for retrieving atmospheric water-vapor and cloud liquid-water paths from the ground [e.g., *Staelin*, 1966; *Westwater*, 1978; *Peter and Kämpfer*, 1992; *Mätzler and Morland*, 2009]. The retrieval algorithms make use of the different spectra of vapor and liquid absorption. Here the focus is on the influence of cloud temperature on retrieval of the liquid-water path. Liquid-water clouds exist over a temperature range covering at least 240 to 300 K. For modeling active and passive microwave signatures of clouds, we need accurate values of the dielectric constant of water over the full range. As noted by *Lin et al.* [2001], the uncertainty of dielectric properties leads to discrepancies between in situ and microwave radiometer data on cloud liquid water, with the largest deviations for supercooled clouds. Unfortunately, the existing dielectric measurements are concentrated at room temperature. One laboratory data set was obtained at the microwave frequency of 9.6 GHz and temperatures down to -18°C [*Bertolini et al.*, 1982], and *Risman and Wäppling-Raaholt* [2007] published measurements at the radio frequency of 925 MHz and temperatures down to -15°C . The available data were used to construct dielectric models of water, which have been applied to clouds over a broad frequency and temperature range. Among the models currently used are those of *Liebe et al.* [1991, 1993], *Stogryn et al.* [1995], *Meissner*

and *Wentz* [2004], *Ellison* [2006, 2007], and *Risman and Wäppling-Raaholt* [2007]. We show in Figure 2 that cloud absorption resulting from these models is consistent at temperatures above 270 K but deviates at lower temperatures, with discrepancies of more than a factor of 2 at 245 K. The deviations directly transform to uncertainties in the liquid-water path. The latter point was also discussed by *Lipton et al.* [1999].

[3] Supercooled clouds are a hazard for aircraft operations [*Rasmussen et al.*, 1992]. Also, the cloud liquid-water path is one of the important parameters determining cloud albedo and, hence, impacts the transmission and reflection of both long-wave and short-wave radiative flux and inference of cloud parameters in climate studies [*Sengupta et al.*, 2003; *Shupe and Intrieri*, 2004]. *Marchand et al.* [2003] discuss the impact of errors in the liquid-water path on inferred cloud radiative properties.

[4] In the present work we report on experimental data on cloud absorption in the 21 to 31 GHz range obtained from ground-based microwave radiometry of the atmosphere. Owing to the lack of independent information on cloud liquid water, we examine ratios of cloud opacity at two frequencies. In this way the liquid-water path is canceled, allowing us to focus on the temperature dependence of these ratios.

[5] The frequency range allows the application of the Rayleigh approximation, and thus the drop-size distribution is irrelevant as long as large drizzle (droplet diameter larger than 0.2 mm) and raindrops are absent. This condition usually applies at temperatures below 273 K. The first description of the method to extract cloud-absorption ratios was presented by *Mätzler and Morland* [2009] together with results from two cloud scenes. The method has since been improved and applied to many events in the temperature

¹Institute of Applied Physics, University of Bern, Bern, Switzerland.

²Research Laboratory of Electronics, Massachusetts Institute of Technology, Cambridge, Massachusetts, USA.

³Institute for Atmospheric and Climate Science, ETH, Zurich, Switzerland.

range from 246 to 279 K. The data confirm the earlier impression that most models represent cloud absorption at low temperatures poorly. However, it is shown here that the model of *Stogryn et al.* [1995; also described in *Wang, 2002*] fits our observations. After describing the data in section 2 and the methods in section 3, we present and discuss the results in section 4, including a comparison with published dielectric data on water. The conclusion is given in section 5. Additional information can be found in a related research report [*Mätzler et al., 2010*].

2. Data

[6] Between January 2006 and February 2010, we observed 76 cloud episodes in Bern, which typically lasted for 1 to 3 h. Only 12 episodes occurred before November 2007, when the 22 GHz data were not yet available (see the following).

2.1. Surface-Based Observations

[7] Microwave data (January 2006 to February 2010) are calibrated brightness temperatures from the Tropospheric Water Radiometer (TROWARA) located in Bern. They include continuous observations of the sky in a constant view direction (SE direction; zenith angle, 50°), with a beam width of 4° for the microwave channels and 2.8° for the infrared channel and a sampling period varying from 1.2 to 1.8 s. TROWARA consists of three microwave channels, at frequencies (including bandwidths, in parentheses) of 21.38 GHz (100 MHz), 22.24 GHz (400 MHz), and 31.5 GHz (200 MHz), and a Heitronics KT 15.85 D infrared radiometer (wavelength range, 9.7–11.5 μm) for measurement of the cloud-base temperature. Microwave radiometer noise levels are approximately 0.05 K for 10 s integration. Since 2002, TROWARA has been operated in a temperature-controlled room with the antennae looking through a Styrofoam window; the 22 GHz channel was added in November 2007. Attention was paid to the requirement of a common beam direction and beam width at all three microwave frequencies to make sure that the same atmospheric features were seen in all channels simultaneously. More details on TROWARA are given by *Peter and Kämpfer* [1992], *Ingold* [2000], *Morland* [2002, 2007], and *Mätzler and Morland* [2008, 2009].

[8] Data from a collocated weather station include air temperature, humidity, pressure, wind, visibility, and precipitation.

2.2. Satellite Data

[9] One source of cloud-top temperatures, T_{top} , was the Atmospheric Infrared Sounder (AIRS) and Advanced Microwave Sounding Unit (AMSU) instruments on the Aqua satellite. The temperature retrieval algorithm combines the infrared and microwave data and is described by *Susskind et al.* [2003, 2006]. We used Version 5 retrievals. Cloud-top temperatures are retrieved for up to two cloud layers, which may partly overlap. The retrieval is done at the spatial resolution of the AMSU, which is 45 km for beam positions near the nadir but increases toward the ends of the instrument's scan. With each temperature retrieval there is an associated $3 \times 3 \times 2$ array of cloud-layer fractions, corresponding to the AIRS spatial resolution of 15 km at nadir and the two cloud layers. The cloud-top temperature was

taken from the retrieval closest to the location of Bern, at the satellite overpass time closest to each TROWARA observation of a supercooled cloud. In cases where the cloud-fraction parameter indicated that two cloud layers were present over the vicinity of Bern, we assumed that the T_{top} of the supercooled liquid layer was the one closest to TROWARA's measurement of the cloud-base temperature; normally, that was the lower-altitude layer.

[10] Another estimate of the T_{top} was obtained from the Moderate Resolution Imaging Spectroradiometer (MODIS) cloud product. Data collected by the instrument aboard the Aqua satellite were used to ensure collocation with AIRS and AMSU (MYD06, collection 5.1). The cloud product is available at a nominal spatial resolution of 5×5 km; a full description is given by *Platnick et al.* [2003]. For the purpose of this study the cloud-top temperature product and the brightness temperatures at 8.5 and 11 μm were used to estimate the T_{top} of the uppermost cloud layer. Data were extracted from each relevant scene for the MODIS pixel within which Bern is located. The mean area of the pixel in the cases considered was 45 km²; the average distance of Bern from the pixel center was 3.2 km.

3. Method

3.1. Estimating the Cloud Temperature

[11] The cloud-base temperature T_{base} was estimated from TROWARA's infrared brightness temperature observed over periods of 5 min each. The maximum temperature was selected to maximize beam filling and opacity. The mean value of T_{base} was taken over the duration of a cloud episode, typically lasting for 1 to 3 h around the time of the satellite overpass.

[12] The mean cloud temperature T was usually assumed to be the mean value of T_{base} and T_{top} . In 60% of the scenes the T_{top} data from MODIS corresponded to those from AIRS-AMSU within 5 K. In 76% of all episodes the TROWARA cloud-base temperature minus the AIRS-AMSU cloud-top temperature was in the reasonable range of between -1 and $+8$ K. Differences of 14 K or more were found in only four cases. More outliers were present in the MODIS data. In situations with contradicting satellite data, values closer to the TROWARA data were assumed to be correct. As shown in the data table (Appendix A5) of *Mätzler et al.* [2010], the MODIS and AIRS-AMSU data turned out to be good complements.

[13] In 15% of the episodes no satellite data were representative for the local clouds. This happened, for instance, when the clouds were too small and the satellite retrievals corresponded to the surface temperature or when ice clouds were present at higher altitudes. In the AIRS-AMSU retrievals the problem of cirrus was almost always avoided by the two-layer solution. If the available satellite data deviated by more than 8 K from $T_{\text{base}} - 3$ K, additional information was used to estimate the mean cloud temperature from the surface-based data alone: The difference between the T_{base} and the surface air temperature was helpful for estimating the potential influence of the atmosphere on the brightness temperature, also using information on water vapor and cloud liquid water. For each episode an error of T was subjectively estimated from the available data. It ranged from 1 to 8 K, with a mean value of 2.5 K.

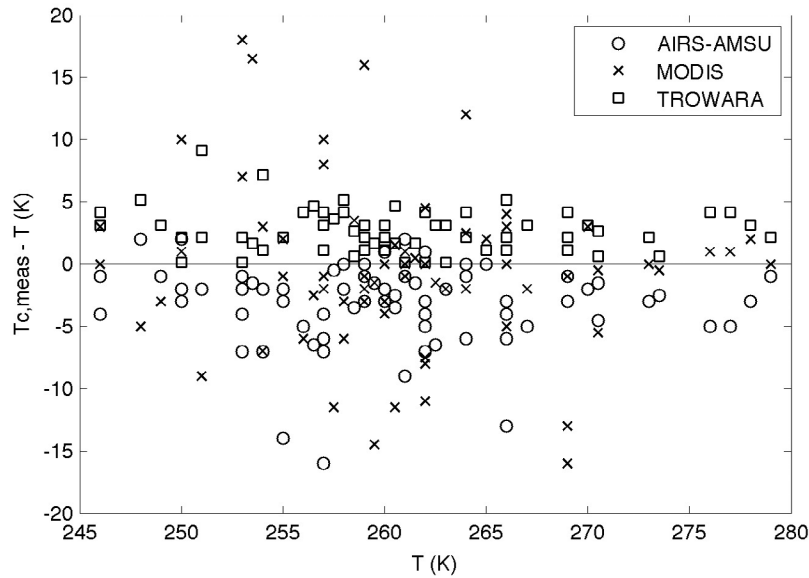


Figure 1. Differences between measured cloud temperatures ($T_{c,\text{meas}}$) from the Atmospheric Infrared Sounder-Advanced Microwave Sounding Unit (AIRS-AMSU) (circles), Moderate Resolution Imaging Spectroradiometer (MODIS) (crosses), and Tropospheric Water Radiometer (TROWARA) (squares) and the estimated mean cloud temperature T_c plotted versus T .

This error is acceptable in view of the temperature sensitivity of the absorption ratios introduced in the following.

[14] A comparison of the differences between cloud temperature data among MODIS, AIRS-AMSU, and TROWARA, and the estimated mean cloud temperatures T are shown versus T in Figure 1. Because TROWARA looks from below, the squares mostly have positive values, whereas the differences from satellite data are mostly negative.

3.2. Opacity

[15] The observed brightness temperature at frequency ν is converted to the slant-path opacity τ as described by Mätzler and Morland [2009]. During periods without precipitation τ is a sum of three terms

$$\tau(\nu) = a(\nu) + \int_0^{\text{TOA}} \rho_V(s) \alpha_V(\nu, s) ds + \int_0^{\text{TOA}} \rho_L(s) \alpha_L(\nu, s) ds, \quad (1)$$

where $a(\nu)$ is the opacity of the dry atmosphere, and the integrals are taken over the propagation path from the radiometer position at $s = 0$ to the top of the atmosphere. Here ρ_V and α_V are the density and mass absorption coefficient of water vapor, and ρ_L and α_L are the respective quantities of cloud liquid water.

[16] Figure 2a shows α_V and α_L at 21.38 GHz (top) and 31.5 GHz (bottom) versus T for different dielectric models of liquid water and the model of Rosenkranz [1998, 1999] for water vapor. Figure 2b shows the spectrum of α_L at $T = 250$ K. For $T > 270$ K all models agree very well, but for lower temperatures the differences in α_L among the models become apparent. Most models in Figure 2 comprise two Debye relaxation terms, with a primary Debye relaxation frequency $\nu_{D,1} \cong 10$ GHz at 0°C , but the model of Ellison [2007] also includes a third term, while the model of Risman and Wüppling-Raaholt [2007] uses only the primary relax-

ation term. The model of Stogryn *et al.* [1995] displays the strongest decrease in cloud opacity for temperatures below 250 K. This behavior is largely due to a strong decrease in $\nu_{D,1}$ (shown, e.g., in Figure 4 of Meissner and Wentz [2004]), which is the effect of two zeros, located at -45° and -49.25°C , in Stogryn and coworkers' expression for that parameter. The second relaxation frequency, $\nu_{D,2}$, in their model was assumed to be independent of temperature. A more physical model would also reduce $\nu_{D,2}$ at very low temperature. This alternative was chosen by inserting $\nu_{D,1}$ from Stogryn *et al.* [1995] into the model of Ellison [2006]; this new model is called ES (for Ellison-Stogryn). Other properties of water, such as heat capacity, compressibility, and expansion coefficient, also undergo rapid changes as the temperature drops below 0°C [Debenedetti and Stanley, 2003; Angell, 2008].

[17] The retrieval algorithms for water vapor and liquid water make use of the different spectra of vapor and liquid absorption [Mätzler and Morland, 2009]. As shown in Figure 2b, at 250 K the dielectric models of Stogryn *et al.* [1995] and ES have flatter absorption spectra in the 20–40 GHz range than any of the others. When used in a retrieval algorithm, a flatter spectrum per unit mass would require higher values of inferred liquid water to fit the observations than for the other models.

[18] With the radiometer frequency now represented by index i , the opacity τ_i can also be expressed by path-averaged values of the mass absorption coefficients b_i and c_i through

$$\tau_i = a_i + b_i V + c_i L, \quad (2)$$

where

$$V = \int_0^{\text{TOA}} \rho_V(s) ds \quad \text{and} \quad L = \int_0^{\text{TOA}} \rho_L(s) ds \quad (3)$$

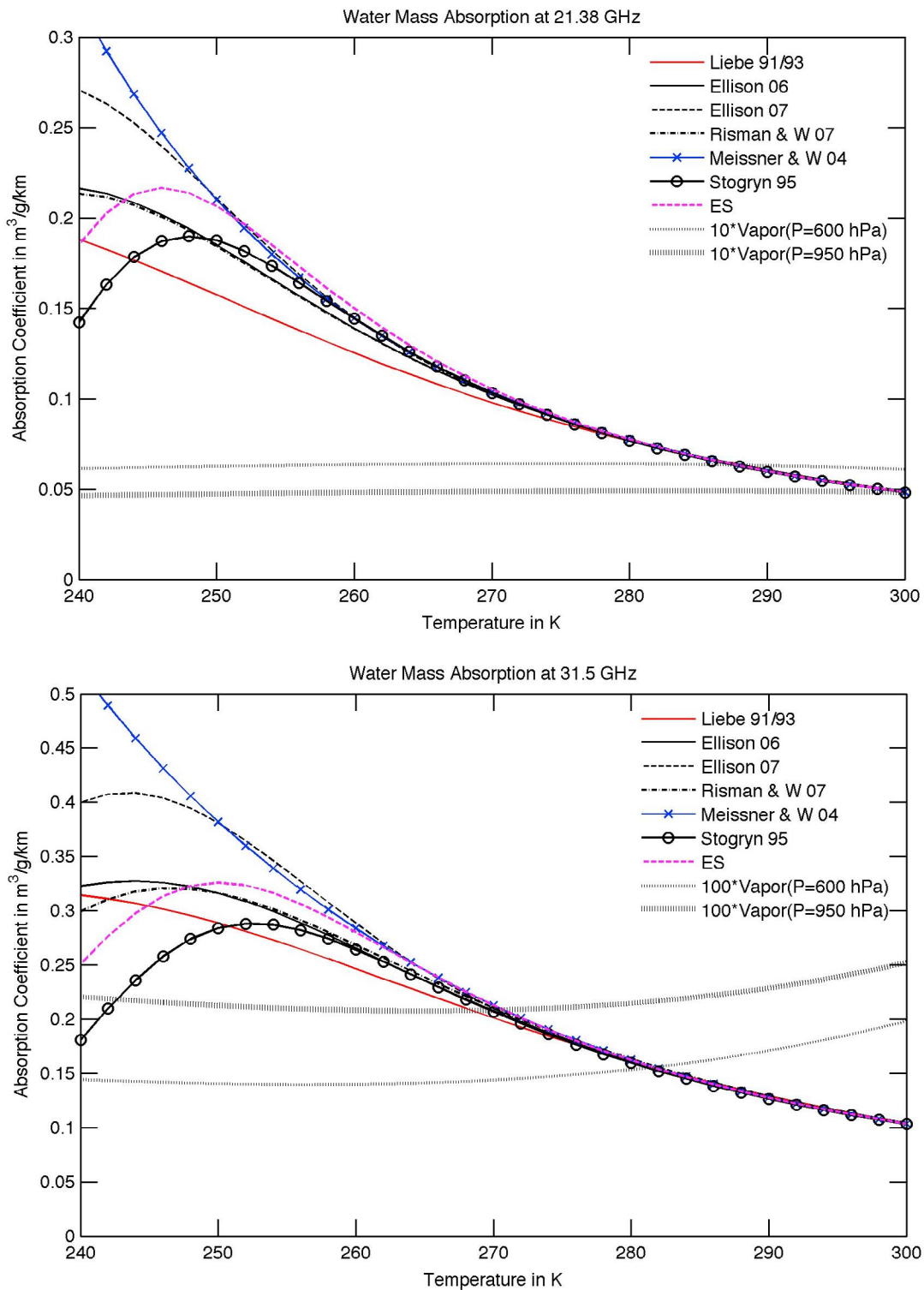


Figure 2. (a) Mass absorption coefficients at 21.38 GHz (top) and at 31.5 GHz (bottom) versus temperature of liquid-water clouds, for different dielectric models of water, and of water vapor, enhanced by a factor of 10 (top) or 100 (bottom) at two selected air pressures (600 and 950 hPa). (b) Mass absorption coefficient versus frequency of liquid-water clouds at $T = 250$ K for the different models. ES: *Stogryn et al.* [1995] and *Ellison* [2006] models combined.

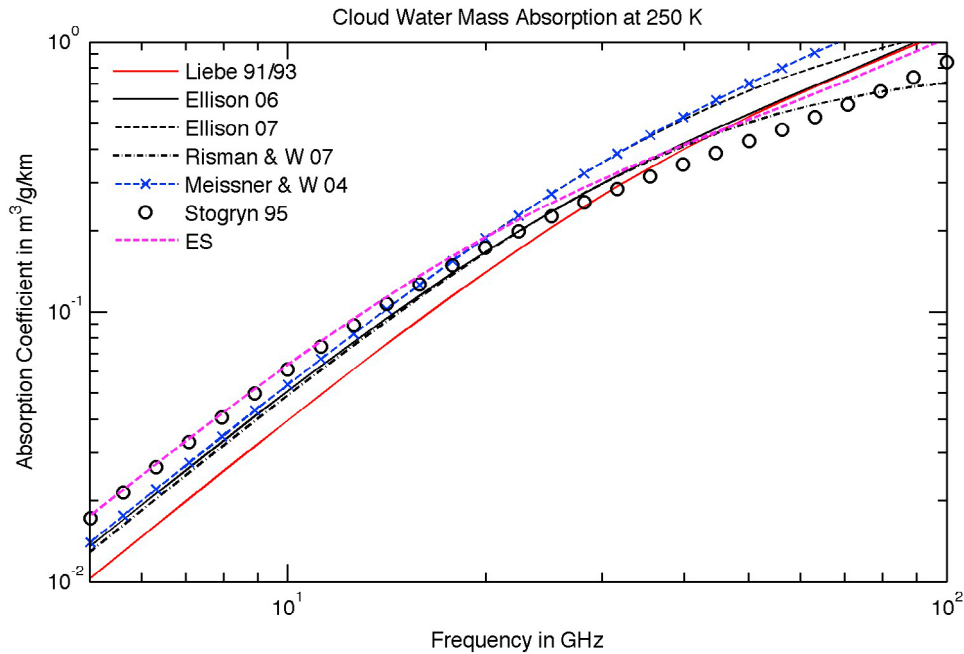


Figure 2. (continued)

are the path-integrated densities of water vapor and liquid water, respectively. Our method concentrates on the temperature dependence of α_L or c_i , respectively. This quantity is independent of the drop-size distribution in the Rayleigh approximation, which is valid in the present frequency range for drop diameters up to 0.2 mm [Mätzler and Morland, 2008]. Plotting the opacities at one of the lower frequencies (21 or 22 GHz) versus the opacity at the higher frequency (31 GHz), the different spectral characteristics of vapor and liquid water make it possible to distinguish among the different processes leading to temporal changes. In this way it became obvious that the variations of cloud water (L) are fast, with typical time scales of the order of 1 min, whereas the larger variations of V are slower, with typical time scales of the order of 1 h or more [Mätzler and Morland, 2009]. As an example, the behavior of the curves on 10 April 2009, 1200–2100 UT, is plotted in Figure 3. A long period was selected to show effects of the slow V variations also. They are represented by the steep and noisy part of the curves. The transition to flatter slopes is due to the occurrence of liquid clouds. We know that these clouds must contain liquid water because in nonprecipitating clouds, absorption by ice particles is negligible at TROWARA's frequencies. Each point represents the average over a time period of about 10 s, and subsequent points are connected by straight lines. Thus long straight lines mean fast and large variations. The given values of the slopes correspond to the fast variations and thus to the measured $\gamma_{i,j}$ ratios described in the following.

3.3. Ratio of Fast Opacity Changes

[19] The Rayleigh formula for the mass absorption coefficient of a water cloud consisting of spherical droplets, in units

of $1/(\text{km} \cdot \text{g}/\text{m}^3)$ and assuming a water density of $1000 \text{ kg}/\text{m}^3$, is given by

$$\alpha_L = 3 \times 10^{-3} k_0 \times \text{Im} \left(\frac{\varepsilon - 1}{\varepsilon + 2} \right) = 9 \times 10^{-3} k_0 \frac{\varepsilon''}{|\varepsilon + 2|^2}, \quad (4)$$

where $\varepsilon = \varepsilon' + i\varepsilon''$ is the complex, relative dielectric constant and k_0 is the vacuum wave number at frequency ν . Given that all antenna beams observe the same atmospheric volume, and assuming that the fast opacity changes $\Delta\tau_i$ are due to changes in cloud liquid alone, we have $\Delta\tau_i = c_i \Delta L$. Because the change observed by the instrument usually happens in a limited volume of a single cloud, the observed absorption change can also be associated with a constant temperature T of this cloud, which means that $\alpha_{L,i}$ is constant along the path, and therefore $c_i = \alpha_{L,i}$. The ratios of such changes at different frequencies are independent of ΔL and, thus, identical to the respective ratios of cloud-absorption coefficients:

$$\gamma_{i,j} = \frac{\Delta\tau_i}{\Delta\tau_j} = \frac{\alpha_{L,i}}{\alpha_{L,j}}; \quad i = 21 \text{ or } 22, \quad j = 31. \quad (5a)$$

Here i and j stand for the rounded frequency in gigahertz, and $\Delta\tau_i$ is the sum of the absolute values of the fast opacity changes exceeding defined thresholds within the time period of the cloud episode (the caption to Figure 3 gives an example). We tried to balance the number of positive and negative opacity changes by slightly changing the threshold and/or time period, to minimize effects resulting from drifts due to slowly varying amounts of water vapor. The uncertainty of the measured $\gamma_{21,31}$ values was estimated for each episode by varying the opacity thresholds, the integration time, and the start and stop time of the episode. The estimated

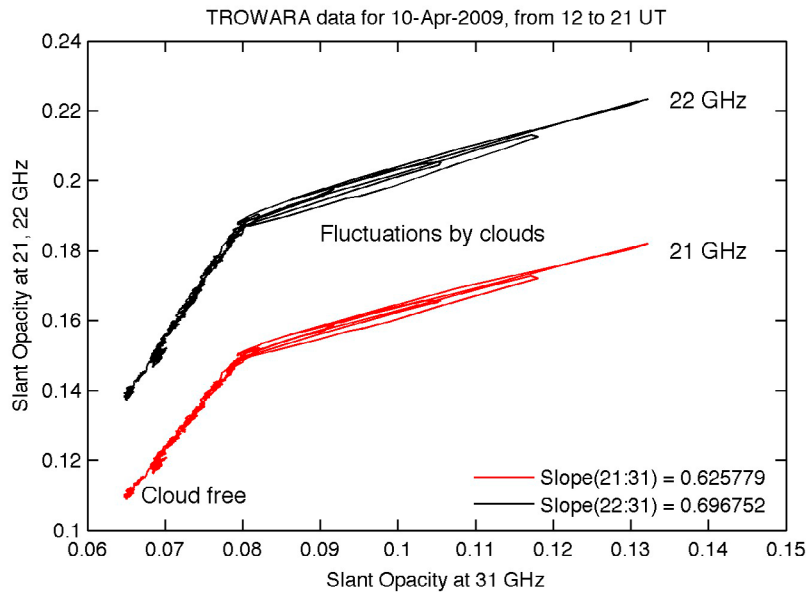


Figure 3. Observed TROWARA slant opacities at 21 GHz (red) and 22 GHz (black) versus slant opacity at 31 GHz on 10 April 2009 from 1200 to 2100 UT. Subsequent measurements are connected by black and red lines, respectively. Values shown for the slopes are weighted averages with simultaneous opacity changes exceeding 0.003 at 21 GHz and 0.0054 at 31 GHz.

errors ranged from 0.002 to 0.02, with a mean value of 0.008. The errors in $\gamma_{22,31}$ are larger, owing to the enhanced influence of water vapor.

[20] The fast changes result either from air parcels with variable cloud amounts moving through the antenna beam or from cloud growth and decay with time. The question arises whether the assumption of a constant V is fully justified and, if not, how large the possible influence of correlated L and V changes is. An estimate of this influence can be obtained from Figure 2a, which shows the mass absorption coefficients versus temperature for both liquid water and water vapor. We find that in terms of mass absorption at 31 GHz, the coefficient of liquid water is about 100 times larger than the coefficient of water vapor. At the lower frequencies, 21 and 22 GHz, the dominance of cloud absorption is smaller but still prevails. Therefore changes in water vapor of the order of the changes in liquid water cannot strongly affect the observed absorption ratios. To quantify this influence we estimated the observed ratios for the assumption of constant total water ($V + L = \text{const}$) during the observed opacity changes. Then the resulting ratio is given by

$$\gamma_{i,j,-} = \frac{\Delta\tau_i}{\Delta\tau_j} = \frac{\alpha_{L,i} - \alpha_{V,i}}{\alpha_{L,j} - \alpha_{V,j}}; \quad i = 21 \text{ or } 22, \quad j = 31. \quad (5b)$$

This situation can occur due to cooling and heating during the growth and decay phases of a cloud. Contrarily, it can be argued that for moving air parcels, the cloud amount should be positively correlated with V . Then we have situations with positive signs of the vapor terms,

$$\gamma_{i,j,+} = \frac{\Delta\tau_i}{\Delta\tau_j} = \frac{\alpha_{L,i} + p\alpha_{V,i}}{\alpha_{L,j} + p\alpha_{V,j}}; \quad i = 21 \text{ or } 22, \quad j = 31, \quad (5c)$$

where $p = \Delta V/\Delta L$ is the ratio of the correlated changes in V to those in L . Equation (5c) is a generalization of equations (5a) and (5b). By choosing $p = 0$, we get the former, and the latter is obtained for $p = -1$. Positive values of p may actually be larger than +1 because, in most circumstances, $V \gg L$. Equation (5c) should also hold in situations of mixed-phase clouds under the action of the Bergeron-Findeisen process [Schwarzenböck *et al.*, 2001]. It occurs for ice supersaturation if the relative humidity with respect to liquid water is below 100%. The evaporation of cloud droplets allows for the rapid growth of ice crystals at an essentially constant vapor density, meaning that $p = 0$. Note that microwave radiometers at frequencies below 90 GHz are insensitive to cloud ice.

4. Results and Discussion

[21] The ratios $\gamma_{21,31}$ versus mean cloud temperature for all scenarios are shown in Figure 4 together with the ratios computed according to equations (5a)–(5c), using the dielectric model of Stogryn *et al.* [1995] for cloud water and the Rosenkranz [1998, 1999] model for water vapor at an air pressure of 800 hPa. The choice of the water-vapor model influences the relative offsets of the “Stogryn+” and “Stogryn–” curves but not the position of the central curve or the data points in Figure 4. It appears that a majority of data points is within the range of the two curves called Stogryn– and Stogryn+, corresponding to equations (5b) and (5c), here with $p = +2$. As a consequence of the increasing influence of water vapor, the difference between the curves increases with T , especially for $T > 260$ K. Data points outside the described range exist at low temperatures, especially at $T < 265$ K. Nevertheless, as the first result from Figure 4 we find that the curves explain the general behavior

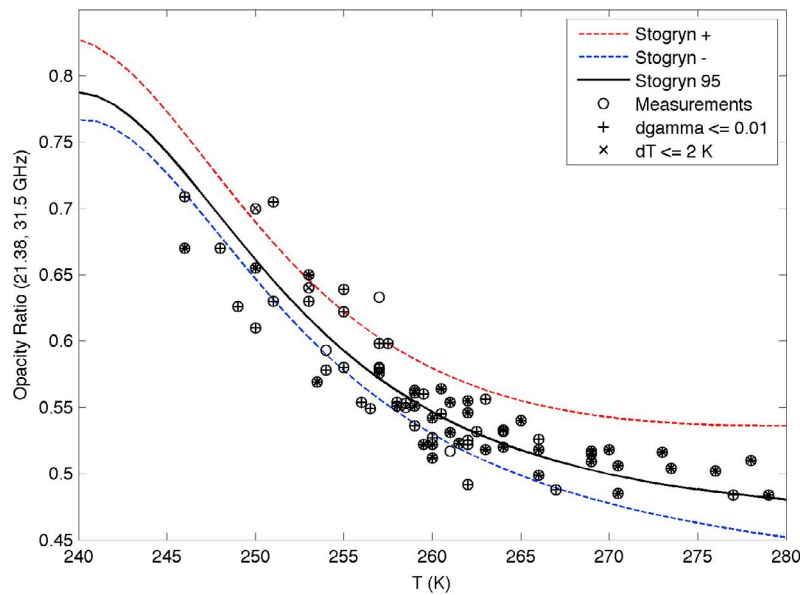


Figure 4. Temperature dependence of the $\gamma_{21,31}$ ratio for the dielectric model of *Stogryn et al.* [1995], equation (5a) (solid (black) line), equation (5b) (dashed blue line), and equation (5c) for $p = +2$ (dashed red line), and compared with measured opacity ratios (circles) and additional qualifiers referring to the estimated errors: $d\gamma$ for the measured ratio and dT for T .

very well. As we will see, such a good agreement is not observed for most of the other dielectric models.

[22] As the second result from Figure 4 we find that correlated water-vapor variations occur together with the rapid changes in cloud water. This is based on the fact that a large fraction of the measurements is contained within the Stogryn- and Stogryn+ curves (difference of ~ 0.05),

whereas the measurement error $d\gamma$ of $\gamma_{21,31}$ is smaller, that is, often less than 0.01. Further insight into the opacity ratios is possible if we compare the γ_{ij} values for different frequency combinations, because the influence of water vapor is different at 21 and 22 GHz.

[23] The equivalent of Figure 4, but for the ratio $\gamma_{22,31}$, is shown in Figure 5. These values are larger by 5% to 10%,

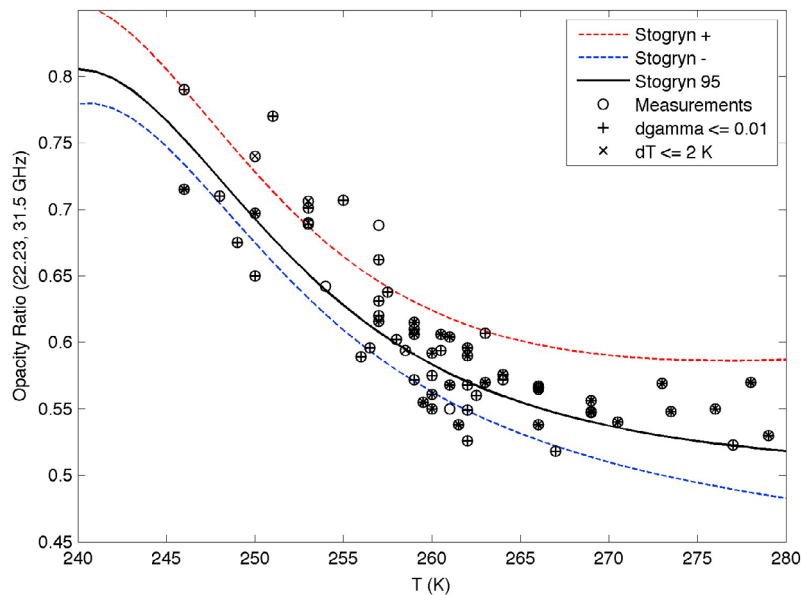


Figure 5. Temperature dependence of the $\gamma_{22,31}$ ratio for the dielectric model of *Stogryn et al.* [1995], equation (5a) (solid (black) line), equation (5b) (dashed blue line), and equation (5c) for $p = +2$ (dashed red line), and compared with measured opacity ratios (circles) and additional qualifiers referring to the estimated errors: $d\gamma$ for the measured ratio and dT for T .

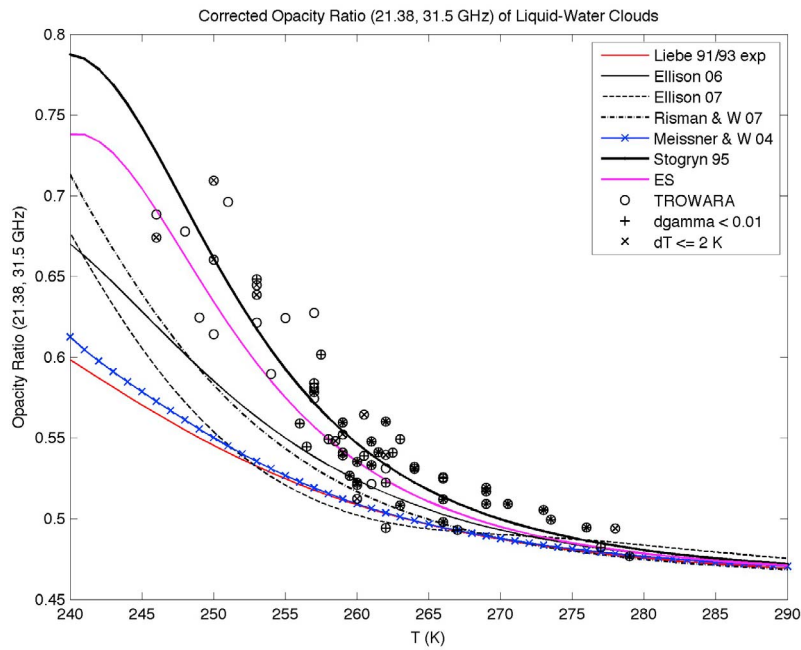


Figure 6. Temperature dependence of the optimized ratios $\gamma_{21,31,opt}$ according to equation (6) for $g = 0.8$ (circles) and additional qualifiers referring to the uncertainties of the ratios and temperatures. Curves represent the cloud-absorption ratios of equation (5) for different dielectric models of water. For details, see figure key and section 4.

the data points scatter more strongly, and the Stogryn+ and Stogryn- curves show larger deviations from the central curve. By using a suitable combination of the ratios $\gamma_{21,31}$ and $\gamma_{22,31}$, the influence of water-vapor fluctuations can be reduced. We used the following combination for the optimized ratio:

$$\gamma_{21,31,opt} = (1 + g)\gamma_{21,31} - 0.93g\gamma_{22,31}, \quad (6)$$

where g is a fitting parameter, and the factor 0.93 is the mean ratio of $\gamma_{21,22} = \gamma_{21,31}/\gamma_{22,31}$.

[24] Optimized ratios according to equation (6) with minimum scatter were found to occur for $g \cong 0.8$. A positive value smaller than unity is expected, as it corrects the water-vapor effect at 21 GHz by a fraction of the stronger effect at 22 GHz. The optimized ratios are shown in Figure 6 together with the results of the different dielectric models. The improvements with respect to the original ratios in Figure 4 are concentrated at $T > 265$ K, where the vapor influence is largest and where the scatter of data points has decreased in Figure 6. At low temperatures, however, the improvement is small.

[25] Another optimization method is described in Appendix A2 of Mätzler *et al.* [2010]. There we tried to quantify the correlated vapor fluctuations individually for each episode. Unfortunately, owing to the relatively large measurement uncertainty of the ratio $\gamma_{21,22}$ and to the pressure dependence of the absorption by water vapor, the method turned out to be inferior to the one in equation (6). Apart from the larger scatter, the results were the same as in Figure 6.

[26] Comparison of the different dielectric models at low temperatures favors that of Stogryn *et al.* [1995], and with

increasing temperature all models converge to the same behavior. The deviation from the measured ratios occurs at $T < 260$ K, most strongly for the model of Liebe *et al.* [1991], which has been popular for many years, as it was included in microwave propagation model MPM93 of Liebe *et al.* [1993]. The term “exp” in the key to Figure 6 refers to the option with an exponential temperature dependence of the relaxation frequency [see Lipton *et al.*, 1999]. Also, the model of Meissner and Wentz [2004] is inappropriate at low temperatures, and a similar conclusion applies to the model of Ellison [2007]. The model of Ellison [2006] is somewhat better, and in the ES model the results are very close to those of Stogryn. This change points to the importance of the main relaxation of liquid water. Halfway between Stogryn and Liebe are the absorption ratios of the single-Debye model of Risman and Wäppling-Raaholt [2007], here extended by the high-frequency limit ϵ_∞ of Okada *et al.* [1997] to take into account its temperature dependence.

[27] Comparing the dielectric models with all available dielectric data, we find that the models of Liebe *et al.* [1991, 1993] and of Risman and Wäppling-Raaholt [2007] have the largest standard deviations. All other models, including that of Stogryn *et al.* [1995], are of comparable quality. This comparison is shown in Table 1 together with the computed opacity ratios at $T = 250$ K for $p = 0$. The temperature range was limited to -10° to $+20^\circ\text{C}$, and the frequency range covered 0.9 to 1000 GHz. Almost twice as many data points are found if the temperature range is extended to $+30^\circ\text{C}$. But the results are essentially the same. Interestingly, the Stogryn *et al.* [1995] and ES models are not optimal compared with the few laboratory measurements of the dielectric constant of supercooled water (Bertolini *et al.* [1982] for 9.61 GHz and Risman and Wäppling-Raaholt [2007] for

Table 1. Comparison of Dielectric Models of Pure Liquid Water: Cloud-Opacity Ratio $\gamma_{21,31}$ at $T = 250$ K for $p = 0$, Standard Deviations (SD), and Mean Values of Real and Imaginary Parts of the Differences Among 363 Measurements of Dielectric Constants (ϵ'_{exp} and ϵ''_{exp}) and the Model Values (ϵ'_{mod} and ϵ''_{mod}), Respectively, in the Temperature Range (-10° to $+20^\circ\text{C}$), Frequency Range (0.9 to 1000 GHz), 90% of Which Are at or Below 100 GHz^a

Model	$\gamma_{21,31}$ at 250 K	SD ($\epsilon'_{\text{exp}} - \epsilon'_{\text{mod}}$)	SD ($\epsilon''_{\text{exp}} - \epsilon''_{\text{mod}}$)	Mean ($\epsilon'_{\text{exp}} - \epsilon'_{\text{mod}}$)	Mean ($\epsilon''_{\text{exp}} - \epsilon''_{\text{mod}}$)
Liebe <i>et al.</i> [1991, 1993]	0.5454	0.8167	0.4118	-0.2397	-0.1108
Ellison [2006]	0.5852	0.5320	0.3699	-0.1013	-0.0706
Ellison [2007]	0.5538	0.5664	0.4331	0.4092	0.0628
Meissner and Wentz [2004]	0.5502	0.5229	0.4084	-0.1095	-0.1281
Risman and Wappling-Raaholt [2007]	0.5827	0.6173	0.6221	-0.2637	-0.1888
Stogryn <i>et al.</i> [1995]	0.6612	0.5412	0.4011	-0.1366	0.0179
Ellison and Stogryn (ES)	0.6342	0.5530	0.4144	0.0487	-0.0800

^aDielectric data on water compiled by Ellison [2007].

925 MHz). Better agreement is found for the model of Meissner and Wentz and the models of Ellison. It should be noted that these models were tuned toward the data of Bertolini *et al.* [1982]. The experimental data sets are compared with the model predictions in Figures 7 and 8. Possible reasons for contradictory results include unexpected errors in the experimental data and unexpected deviations from general assumptions made with respect to cloud particles. That the experimental errors in ϵ' and ϵ'' were underestimated in Bertolini's data was stated by Risman and Wappling-Raaholt [2007], and Angell [1982] pointed to significant artifacts caused by measurements of supercooled water in thin capillary tubes.

[28] Deviations from the assumption of pure water droplets occur by impurities in clouds. An estimate of ionic impurities, using Stogryn's model, shows that cloud droplets consisting of ocean water cause a decrease in the absorption ratio $\gamma_{21,31}$, which changes from 0.02 to 0 over the temperature range from 245 to 280 K. This change is too small and in the wrong direction, implying that ionic impurities cannot explain the model deviation of the absorption ratios from our data at low temperature.

[29] Although highly unrealistic for liquid cloud droplets, deviations of their shape from spheres have a significant influence on cloud absorption. As presented in the Appendix of Matzler *et al.* [2010], droplet axial ratios on the order of 2:1 are required to reconcile an average dielectric model with the measured absorption ratio presented in Figure 6. Alternatives are clouds of spherical droplets consisting of an anisotropic medium. This could happen if supercooled water became ferroelectric. Speculations on such behavior were refuted in an experiment conducted by Hasted and Shahidi [1976].

[30] Our assumption that the mean radiating temperature of liquid in the clouds is the average of base and top temperatures would be violated if ice particles predominated in the colder (higher) part, and liquid predominated in the lower and warmer part of the same cloud layer. Naud *et al.* [2010] measured cloud phase at two midlatitude locations with lidar for the temperature range 233–273 K. They found mixed-phase clouds to be about as common as clouds of uniform phase. At the central U.S. site the maximum supercooled liquid tended to occur within the cloud, while at the French site it tended to peak at the cloud base. If the

latter type of mixed-phase clouds were present in our data, the mean cloud temperature T could have a negative bias of up to a few degrees with respect to the mean temperature of the liquid phase; this would imply that Figure 6 understates the disagreement between the opacity-ratio measurements and most of the dielectric models.

[31] The fact that the present analysis, made in the 20–30 GHz range, is not in harmony with dielectric laboratory measurements of supercooled water at lower frequencies is an argument for more experimental work. On the side of supercooled clouds this work should be extended in frequency down to about 15 GHz and up to about 150 GHz to increase the amount of information that can be gained from microwave radiometers. Regarding future laboratory experiments advances can be expected from numerical solvers of Maxwell's equations adapted to the optimal geometries for keeping water in a supercooled condition, such as in capillary glass tubes [Risman and Wappling-Raaholt, 2007].

5. Conclusions

[32] The present investigations have revealed important results on microwave absorption of supercooled clouds. Ratios $\gamma_{21,31}$ and $\gamma_{22,31}$ of fast opacity changes observed over 4 years at frequency pairs of the TROWARA radiometer system were related to the respective ratios of cloud absorption coefficients in the Rayleigh approximation. The 76 cloud episodes studied covered the temperature range from 246 to 279 K. The temperature variation of the measured absorption ratios agrees with the dielectric water model of Stogryn *et al.* [1995] and with other models using their primary relaxation frequency, whereas the more widely known models of water permittivity are unable to describe the observed behavior at temperatures below about 260 K unless very special assumptions on the shape or on the physical properties of cloud particles are made. Scatter of the absorption ratios was explained by correlated fluctuations of water vapor.

[33] The model of Stogryn *et al.* [1995] and the newly defined ES model are the best ones in view of the data presented. These models are not worse than any other when compared with the available dielectric database of water. Still, laboratory experiments on supercooled water give preference to other models. Clarifications are needed

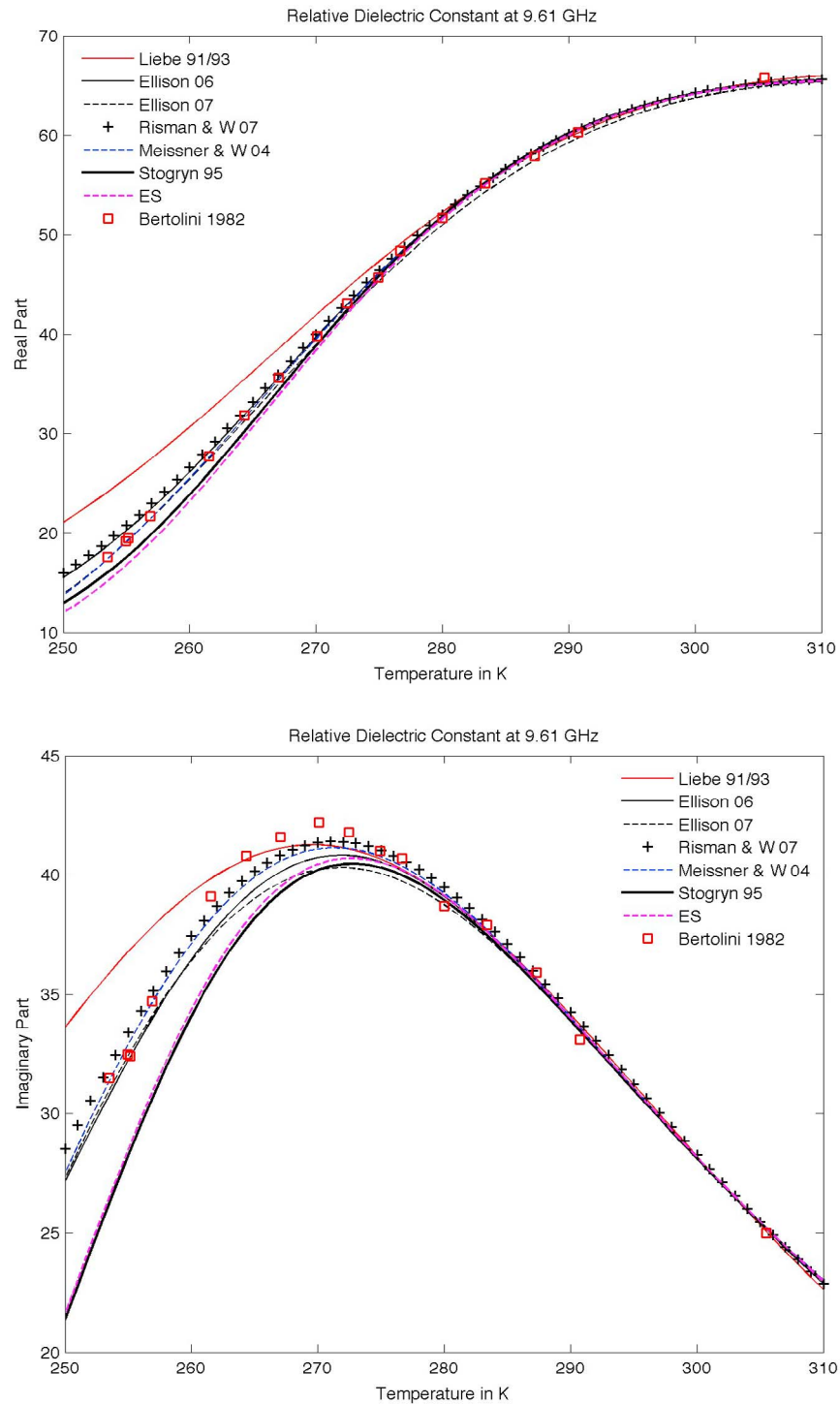


Figure 7. Temperature dependence of the dielectric constant of water at 9.61 GHz: experimental data of Bertolini *et al.* [1982] in comparison with models. (top) Real part; (bottom) imaginary part.

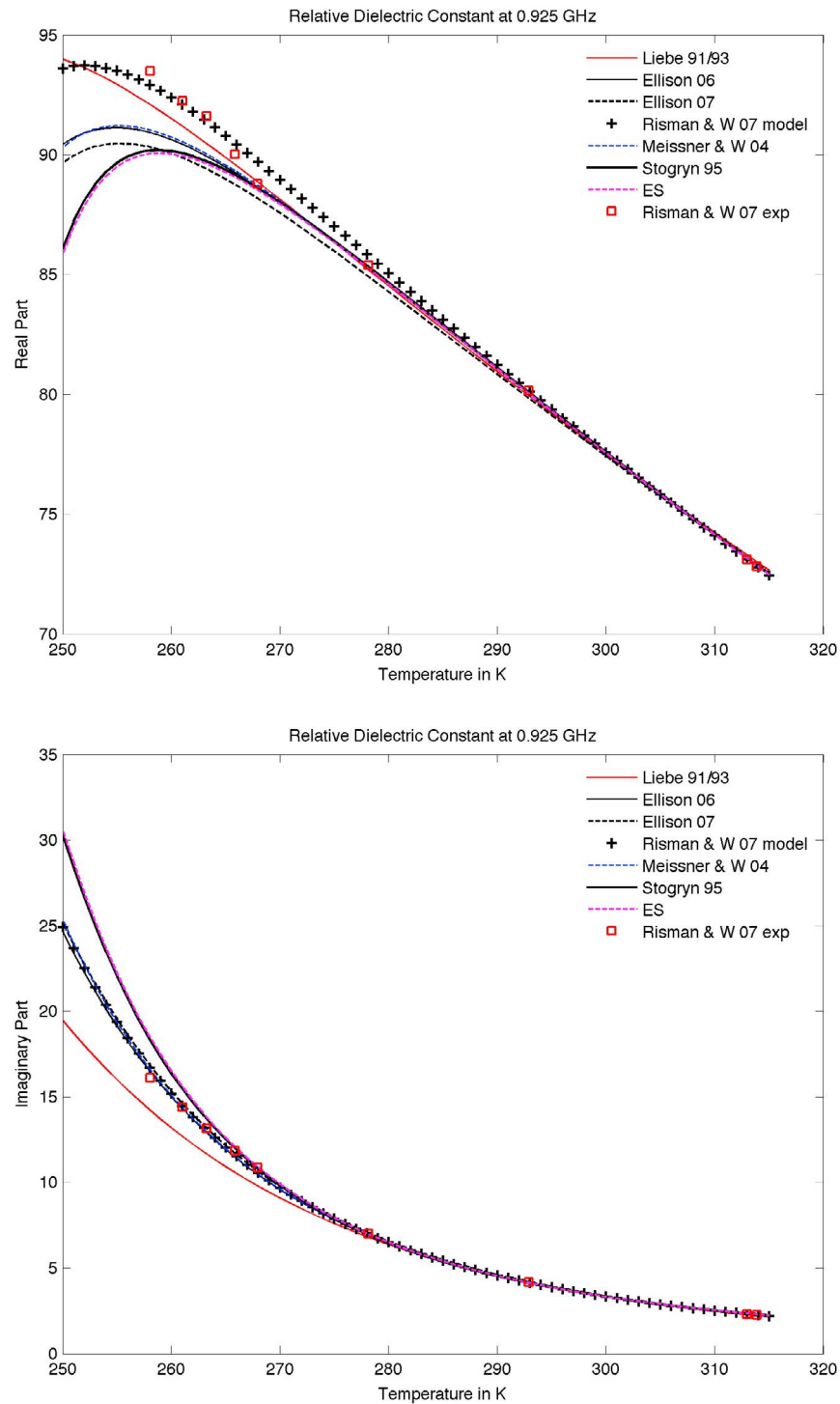


Figure 8. Temperature dependence of the dielectric constant of water at 925 MHz: experimental data of *Risman and Wäppling-Raaholt* [2007] in comparison with models. (top) Real part; (bottom) imaginary part.

through further studies, both in the laboratory and with water clouds. The improved accuracy in these models reduces the uncertainty in the measurements of the cloud-liquid-water path, which is a most relevant cloud property. Better knowledge of the dielectric properties of supercooled water also advances the physics of water.

[34] **Acknowledgments.** The collaboration in this work was supported by LIMAT (<http://lightandmatter.ch/>). We thank three referees for their valuable comments and Thomas Flury for the backward trajectory computation to the time of the satellite overpass for the episode on 27 October 2007. We also thank David Staelin for suggesting improvements on an early version of this paper.

References

- Angell, C. A. (1982), Supercooled water, in *Water—A Comprehensive Treatise: Vol. 7. Water and Aqueous Solutions at Subzero Temperatures*, edited by F. Franks (ed.), chap. 1, Plenum Press, New York.
- Angell, C. A. (2008), Insight into phases of liquid water from study of its unusual glass-forming properties, *Science*, *319*, 582–587, doi:10.1126/science.1131939.
- Bertolini, D., M. Cassettari, and G. Salvetti (1982), The dielectric relaxation time of supercooled water, *J. Chem. Phys.*, *76*, 3285–3290.
- Debenedetti, P. G., and H. E. Stanley (2003), Supercooled and glassy water, *Phys. Today*, June, 40–46.
- Ellison, W. (2006), Freshwater and sea water, in *Thermal Microwave Radiation—Applications for Remote Sensing*, IET Electromagnetic Waves Series 52, edited by C. Mätzler, coedited by P. W. Rosenkranz, A. Battaglia, and J. P. Wigneron, sect. 5.2, Institute of Engineering and Technology, London.
- Ellison, W. (2007), Permittivity of pure water at standard atmospheric pressure, over the frequency range 0–25 THz and the temperature range 0–100°C, *J. Phys. Chem. Data*, *36*(1), 1–17.
- Hasted, J. B., and M. Shahidi (1976), The low-frequency dielectric constant of supercooled water, *Nature*, *262*, 777–778.
- Ingold, T. (2000), Four years of columnar water vapor measurements above the Swiss central plain using radiosondes and a microwave radiometer, *IAP Res. Rep. No. 2000–02*, Institute of Applied Physics, University of Bern, Bern.
- Liebe, H. J., G. A. Hufford, and T. Manabe (1991), A model for the permittivity of water at frequencies below 1 THz, *Int. J. Infrared Millimeter Waves*, *12*, 659–675.
- Liebe, H. J., G. A. Hufford, and M. G. Cotton (1993), Propagation modeling of moist air and suspended water/ice particles at frequencies below 1000 GHz, in *AGARD, 52nd Specialists' Meeting of the Electromagnetic Wave Propagation Panel, Mallorca, Spain*, pp. 3–1–3–10.
- Lin, B., P. Minnis, A. Fan, J. A. Curry, and H. Gerber (2001), Comparison of cloud liquid water paths derived from in situ and microwave data taken during the SHEBA/FIREACE, *Geophys. Res. Lett.*, *28*(6), 975–978.
- Lipton, A. E., M. K. Griffin and A. G. Ling, (1999), Microwave transfer model differences in remote sensing of cloud liquid water at low temperatures, *IEEE Trans. Geosci. Remote Sens.*, *37*(1), 620–623.
- Mätzler, C., and J. Morland (2008), Advances in surface-based radiometry of atmospheric water, *IAP Res. Rep. 2008-02-MW*, University of Bern, Bern, Switzerland.
- Mätzler, C., and J. Morland (2009), Refined physical retrieval of integrated water vapor and cloud liquid for microwave radiometer data, *IEEE Trans. Geosci. Remote Sens.*, *47*(6), 1585–1594.
- Mätzler, C., P. W. Rosenkranz, and J. Cermak (2010), Microwave absorption measurements of supercooled clouds and implications for the dielectric properties of water, *IAP Res. Rep. 2010-02-MW*, Institute for Applied Physics, University of Bern, Bern, Switzerland.
- Marchand, R., T. Ackerman, E. R. Westwater, S. A. Clough, K. Cady-Pereira, and J. C. Liljegren (2003), An assessment of microwave absorption models and retrievals of cloud liquid water using clear-sky data, *J. Geophys. Res.*, *108*(D24), 4773, doi:10.1029/2003JD003843.
- Meissner, T., and F. Wentz (2004), The complex dielectric constant of pure water and sea water from microwave satellite observations, *IEEE Trans. Geosci. Remote Sens.*, *49*(9), 1836–1849.
- Morland, J. (2002), TROWARA—Tropospheric Water Vapour Radiometer. Radiometer review and new calibration model, *IAP Res. Rep. 2002-15*, Institute for Applied Physics, University of Bern, Bern, Switzerland.
- Morland, J. (2007), TROWARA—Rain flag development and stability of instrument and calibration, *IAP Res. Rep. 2007-13-MW*, Institute for Applied Physics, University of Bern, Bern.
- Naud, C. M., A. D. Del Genio, M. Haeffelin, Y. Morille, V. Noel, J.-C. Dupont, D. D. Turner, C. Lo, and J. Comstock (2010), Thermodynamic phase profiles of optically thin midlatitude clouds and their relation to temperature, *J. Geophys. Res.*, *115*, D11202, doi:10.1029/2009JD012889.
- Okada, K., Y. Imashuku, and M. Yao (1997), Microwave spectroscopy of supercritical water, *J. Chem. Phys.*, *107*(22), 9302–9311.
- Peter, R., and N. Kämpfer (1992), Radiometric determination of water vapor and liquid water and its validation with other techniques, *J. Geophys. Res.*, *97*(D16), 18,173–18,183.
- Platnick, S., M. D. King, S. A. Ackerman, W. P. Menzel, B. A. Baum, J. C. Riedi, and R. A. Frey (2003), The MODIS cloud products: Algorithms and examples from Terra, *IEEE Trans. Geosci. Remote Sens.*, *41*, 459–473.
- Rasmussen, R., et al. (1992), Winter Icing and Storm Project (WISP), *Bull. Am. Meteorol. Soc.*, *73*, 951–974.
- Risman, P. O., and B. Wäppling-Raaholt (2007), Retro-modelling of a dual resonant applicator and accurate dielectric properties of water from –20°C to +100°C, *Measure. Sci. Technol.*, *17*, 959–966, doi:10.1088/0957-0233/18/4/001.
- Rosenkranz, P. W. (1998), Water vapor microwave continuum absorption: A comparison of measurements and models, *Radio Sci.*, *33*, 919–928.
- Rosenkranz, P. W. (1999), Erratum, *Radio Sci.*, *34*, 1025.
- Schwarzenböck, A., S. Mertes, J. Heintzenberg, W. Wobrock and P. Laj (2001), Impact of the Bergeron–Findeisen process on the release of aerosol particles during the evolution of cloud ice, *Atmos. Res.*, *58*, 295–313.
- Sengupta, M., E. E. Clothiaux, T. P. Ackerman, S. Kato, and Q. Min (2003), Importance of liquid water path for estimation of solar radiation in warm boundary layer clouds: An observational study, *J. Climate*, *16*, 2997–3009.
- Shupe, M. D., and J. M. Intrieri (2004), Cloud radiative forcing of the Arctic surface: The influence of cloud properties, surface albedo, and solar zenith angle, *J. Climate*, *17*, 616–628.
- Staelin, D. H. (1966), Measurements and interpretation of the microwave spectrum of the terrestrial atmosphere near 1-cm wavelength, *J. Geophys. Res.*, *71*, 2875–2881.
- Stogryn, A. P., H. T. Bull, K. Rubayi, and S. Iravanchy (1995), The microwave permittivity of sea and fresh water, *Aerojet Internal Rep.*, Aerojet, Sacramento, Calif.
- Susskind, J., C. D. Barnet, and J. M. Blaisdell (2003), Retrieval of atmospheric and surface parameters from AIRS/AMSU/HSB data in the presence of clouds, *IEEE Trans. Geosci. Remote Sens.*, *41*(2), 390–409.
- Susskind, J., C. Barnet, J. Blaisdell, L. Iredell, F. Keita, L. Kouvaris, G. Molnar, and M. Chahine (2006), Accuracy of geophysical parameters derived from Atmospheric Infrared Sounder/advanced microwave sounding unit as a function of fractional cloud cover, *J. Geophys. Res.*, *111*, D09S17, doi:10.1029/2005JD006272.
- Wang, J. R. (2002), A comparison of the MIR-estimated and model-calculated fresh water surface emissivities at 89, 150, and 220 GHz, *IEEE Trans. Geosci. Remote Sens.*, *40*(6), 1356–1365.
- Westwater, E. R. (1978), The accuracy of water vapor and cloud liquid determination by dual-frequency ground-based microwave radiometry, *Radio Sci.*, *13*(4), 677–685.

J. Cermak, Institute for Atmospheric and Climate Science, CHN, Universitätstr. 16, ETH Zurich, CH-8092 Zurich, Switzerland.

C. Mätzler, Institute of Applied Physics, University of Bern, Sidlerstrasse 5, CH-3012 Bern, Switzerland. (matzler@iap.unibe.ch)

P. W. Rosenkranz, Research Laboratory of Electronics, Massachusetts Institute of Technology, Cambridge, MA 02142, USA.